RESEARCH ARTICLE | FEBRUARY 06 2023

Active stabilization of a pseudoheterodyne scattering scanning near field optical microscope

David Becerril [ID] ; Tiziana Cesca; Giovanni Mattei; Cecilia Noguez [✉] [ID] ; Giuseppe Pirruccio [✉] [ID] ; Marco Luce [ID] ; Antonio Cricenti [✉] [ID]

Check for updates

CrossMark

View Online   Export Citation

Active stabilization of a pseudoheterodyne scattering scanning near field optical microscope
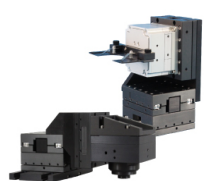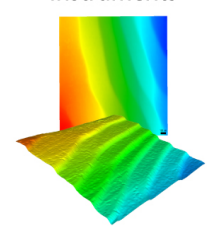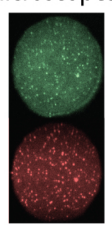
View Online Export Citation CrossMark

David Becerril,[1,2] Tiziana Cesca,[3] Giovanni Mattei,[3] Cecilia Noguez,[2,a] Giuseppe Pirruccio,[2,a]
Marco Luce,[1] and Antonio Cricenti[1,a]

AFFILIATIONS

[1]Istituto di Struttura della Materia, Consiglio Nazionale delle Ricerche (CNR), Via Fosso del Cavaliere 100, 00133 Rome, Italy
[2]Instituto de Fisica, Universidad Nacional Autonoma de Mexico, Apartado Postal 20-364, Ciudad de Mexico 01000, Mexico
[3]Department of Physics and Astronomy, University of Padova, Via Marzolo 8, I-35131 Padova, Italy

[a]Authors to whom correspondence should be addressed: cecilia@fisica.unam.mx; pirruccio@fisica.unam.m;
and antonio.cricenti@artov.ism.cnr.it

ABSTRACT

Scattering scanning near-field optical microscopes (s-SNOMs) based on pseudoheterodyne detection and operating at ambient conditions typically suffer from instabilities related to the variable optical path length of the interferometer arms. These cause strong oscillations in the measured optical amplitude and phase comparable with those of the signal and, thus, resulting in dramatic artifacts. Besides hampering the comparison between the topography and the optical measurements, such oscillations may lead to misinterpretations of the physical phenomena occurring at the sample surface, especially for nanostructured materials. Here, we propose a stabilizing method based on interferometer phase control, which improves substantially the image quality and allows the correct extraction of optical phase and amplitude for both micro- and nanostructures. This stabilization method expands the measurement capabilities of s-SNOM to any slowly time-dependent phenomena that require long-term stability of the system. We envisage that active stabilization will increase the technological significance of s-SNOMs and will have far-reaching applications in the field of heat transfer and nanoelectronics.

I. INTRODUCTION

Scanning Near-field Optical Microscopy (SNOM) is a commonly used method to overcome the diffraction limit in optical microscopy. Many SNOM setups have been discussed in the literature in which the method of illumination and detection vary. In general, a SNOM setup consists of an atomic force microscope (AFM) coupled to a monochromatic coherent light source, permitting the SNOM to acquire AFM topographic and optical images simultaneously while scanning the sample. The AFM tip is located in the near-field zone, i.e., at distances comparable to the illumination wavelength where evanescent waves couple strongly to the sample and the probe. Since evanescent waves are not held by the diffraction limit as traveling waves are, access to evanescent waves allows the achievement of high resolution. Scattering scanning near-field optical microscopy (s-SNOM) is a particular SNOM method that has attracted massive interest due to its capabilities of probing the optical and chemical properties of samples at high resolutions.[1–5] s-SNOM has been applied at visible wavelengths to a wide range

of materials and applications ranging from inorganic metallic structures used for data storage[6] or plasmon excitations[7] to organic materials and spectroscopic studies on tobacco mosaic viruses, rendering the method a very important tool for material science and biology.[8]

One of the main challenges of s-SNOM detection is the separation of the small near-field signal from the large unwanted background noise produced due to far-field scattering of the incident field from surfaces other than the tip such as the shaft or the sample itself. A second task is to disentangle the amplitude and phase of the scattered electromagnetic (EM) field.

In order to separate the near-field optical amplitude and phase, an interferometric detection can be used, combining the scattered light with a reference beam having a fixed (homodyne) or modulated (pseudoheterodyne) relative phase. It has been shown that the interferometric method increases the sensitivity of the measurement as well as fully eliminates unwanted background signals.[9]

While interferometric detection has many advantages, one of its possible drawbacks is that it is extremely sensitive to mechanical

13 January 2024 00:07:29

instabilities and/or thermal fluctuations, particularly when measurements are carried out at room temperature and atmospheric conditions. Past work has shown that phase control methods can be used to stabilize an interferometer when used in an experimental setup.[10] In particular, phase control has been applied in the homodyne detection scheme by using an auxiliary laser beam, which has a similar optical path as that of the primary beam.[11] In this work, we propose a stabilization technique for a pseudoheterodyne interferometric s-SNOM and demonstrate experimentally not only a clear increase in the stability of the measurement but, most importantly, the elimination of artifacts in the images potentially leading to misinterpretations otherwise hard to detect. By stabilizing the phase of the near-field signal before each scan line, our solution extends the typical measurement time window in which stability is guaranteed from the order of minutes to any required time, therefore allowing the investigation of micrometer-sized samples with nanometric resolution, slowly time-dependent phenomena, or the point-by-point accumulation of intrinsically low optical signal intensities.

II. SCATTERING SNOM WITH ACTIVE STABILIZATION

Our s-SNOM setup consists of a monochromatic coherent light source and a homemade atomic force microscope as can be seen in the schematic of Fig. 1(c). We used a He–Ne laser emitting at 633 nm to align the setup. Several light sources can be coupled to the s-SNOM by means of a fiber based reflective collimator, making the setup achromatic throughout the spectral window in which the optical components are designed for. In this work, we used the mentioned He–Ne laser and a 1.5 μm diode. The light beam coming from the source is split and travels along two arms. One beam is directed toward the AFM, the other is sent to a mirror attached to a piezo-actuator oscillating at frequency ω driven with a voltage V_d. This arm is used to create a phase modulated reference beam in an interferometer. An AFM tip, with a typical radius of about 40 nm, is made to oscillate near the resonant frequency of the cantilever Ω above the sample surface. Linearly p-polarized light is focused onto the tip–sample junction with an angle of about 30° with respect to the sample surface. The spot is produced by focusing the laser beam using a gold coated reflective objective lens, which has been chosen because it covers the visible and infrared spectrum. The entire setup is placed on a Newport optical breadboard, which itself is on a Vh3660w vibration isolation table base. The setup is covered with a plastic homemade isolation box that reduces noise and air currents.

The incident electromagnetic (EM) field is concentrated at the apex of the AFM tip creating an EM hotspot.[12] Light scattered by the tip–sample junction contains information about the local near-field response of the sample. Since the near-field signal depends on the local dielectric function, a contrast arises between regions of different optical properties. Back-scattered light is collected by the objective lens and combined, after the beam splitter, with that of the reference arm of the Michelson interferometer. Because of the interference between the weak electric field scattered by the tip–sample, E_s, and the strong one coming from the reference arm, E_R, the former is amplified. The total electric field $E_s + E_R$ generates a signal u proportional to the light intensity. In the heterodyne scheme, u is modulated at frequencies $n\Omega + m\omega$, where n is a harmonic of the AFM tip and m is a harmonic of the reference mirror frequency.
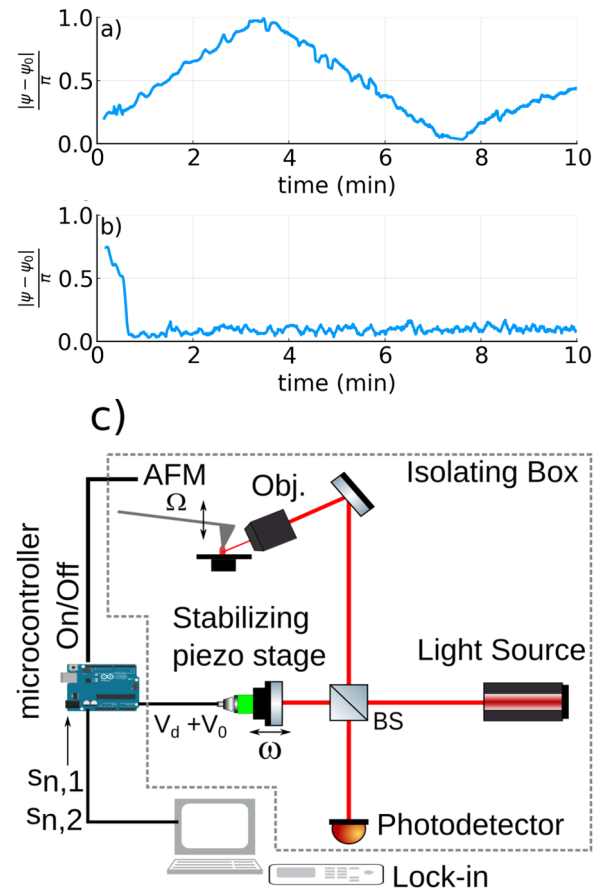
FIG. 1. Absolute value of the phase difference $|\psi - \psi_0|$ with $\psi_0 = \pi$ measured at $n = 2$ vs time inside the isolation box with (a) stabilization mechanism turned "off" and (b) with stabilization turned "on." (c) Schematic of the experimental setup.

It has been shown that lock-in demodulation at high harmonics $n\Omega$ with $n \geq 2$ and at sidebands $m\omega$ reduces unwanted far-field background component.[1]

Detailed mathematical descriptions of the measured signal using a pseudoheterodyne s-SNOM have been given in the literature;[9] for the sake of completeness, we give a brief overview in the supplementary material. The measured signal at harmonic n and sideband m is given by

$$u_{n,m} = 2\kappa\rho J_m(\gamma)s_n \cos(\phi_n - \Psi_R - m\pi/2), \qquad (1)$$

where κ describes the detector sensitivity, ρ is the reference beam intensity, $J_m(\gamma)$ is the Bessel function of the first kind, γ describes the oscillating mirror amplitude, and Ψ_R is the relative path difference between the interferometer beams. The scattered near-field amplitude and phase components are given by s_n and ϕ_n. From Eq. (1), it can be seen that in order to obtain both the amplitude and phase of the near field, it is necessary to measure at two different sidebands. We point out that by simultaneously measuring signals $u_{n,1}$ and $u_{n,2}$, obtained from the lock-in amplifier, we can calculate $\psi = \phi_n - \Psi_R$,

$$\psi \propto \operatorname{atan}\left(\frac{u_{n,1}}{u_{n,2}}\right). \qquad (2)$$

By measuring at a single sample point for different times, we can obtain $\psi(t)$, which describes changes in the optical path difference between the interferometer arms. To obtain the equal sign in Eq. (2), a correct driving frequency V_d must be chosen to satisfy $J_1(\gamma) = J_2(\gamma)$. This is described in the supplementary material.

Due to the mechanical instabilities of our setup and possible thermal fluctuations within the isolating box, we obtain an unstable relative path difference $\psi(t)$. We point out that these fluctuations are present both during acquisition and when the tip is held at one point. Similar fluctuations were also seen when measuring the stability only of the interferometer, by placing a mirror before the beam reaches the objective lens. Therefore, oscillations in the demodulated signal cannot be attributed to interference with far-field waves.

We propose a method to control the phase between the interferometer arms and increase stability in the optical measurements. The stabilization mechanism for the acquisition of an entire image works in the following way: At the beginning of each acquisition line, the phase ψ is calculated and compared to a chosen reference phase ψ_0 via a microcontroller feedback algorithm. A microcontroller output voltage V_o is calculated and sent to the stabilizing piezo that increases or decreases the length of the reference arm to make up for the changes in the optical path. When $\psi - \psi_0$ is calculated up to a given tolerance, the microcontroller halts the stabilization process and sends a signal to the AFM to begin the acquisition of the following row. This process is repeated for each row of the image. Another possible strategy for addressing the stability problem uses the fact that if the oscillating mirror is driven in a way such that $J_1(\gamma) = J_2(\gamma)$ as it is shown in Eq. (2), it is possible to retrieve the amplitude of the optical measurements by calculating $|s_n|^2 = u_{n,1}^2 + u_{n,2}^2$ as is evident from Eq. (1). This procedure was carried out before the development of the stabilization feedback; however, the information on the optical phase is lost.

We point out that the value of ψ_0 can be arbitrarily chosen as it works only as a reference, and stabilization is turned "off" during the data acquisition of the row, allowing for a measurement of the sample phase instead of the chosen reference phase. The program for the microcontroller has been made using standard open source C++ libraries and is available online.[13] In Fig. 1(a), we show the oscillations of the optical path difference over several minutes compared to a reference $\psi_0 = \pi$. In Fig. 1(b), we show the calculated phase difference after switching our stabilization mechanism at "on" $t = 0$.

To test our stabilization mechanism for image acquisition, we use a calibration grating sample NT-MDT TGZ2, which is a groove structure whose top step is composed of SiO_2 and the bottom step of Si. The optical contrast between Si and SiO_2 has been observed using an s-SNOM setup at a similar wavelength of 685 nm as shown in a previous study.[14] In Fig. 2, we show the simultaneously measured topography, optical amplitude, and phase at $n = 2$ and $m = 1, 2$ with the stabilization feedback turned "off." Data acquisition is taken by horizontal rows beginning at the bottom of the image. Slow vertical oscillations in the image can be seen due to the instabilities in the signal, which can be traced back
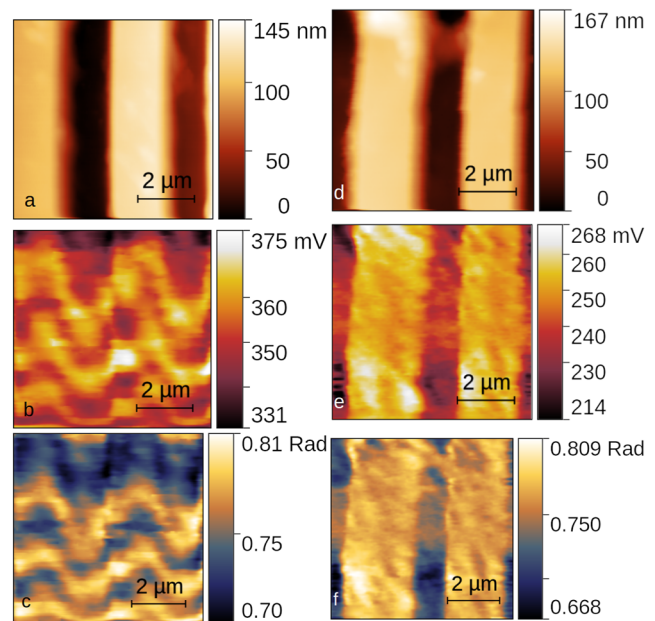

FIG. 2. (a) Topography and optical, (b) amplitude, and (c) phase measured at 2 Ω without stabilization mechanism. (d) Topography and optical, (e) amplitude, and (f) phase measured at 2 Ω with the stabilization mechanism "on."

to changes in the relative optical path between the interferometer arms.

These oscillations completely dominate the measurement, making the contrast between materials unidentifiable and the comparison with the topography impossible. In Fig. 2, we show the same sample measured with the stabilization procedure turned "on." As can be seen, the optical amplitude and phase contrast are clearly visible between the materials, and the slow vertical oscillations are eliminated.

As a further check that we are obtaining correct measurements, we can theoretically estimate the contrast that should be obtained between Si and SiO_2 at an exciting wavelength of 633 nm.[14] This can be done by calculating the effective polarizability of the tip–sample system applying the quasi-static approximation and modeling the tip as a perfect sphere. By taking $\epsilon_{Si} = 14.79 + i0.061$ and $\epsilon_{SiO_2} = 2.119$
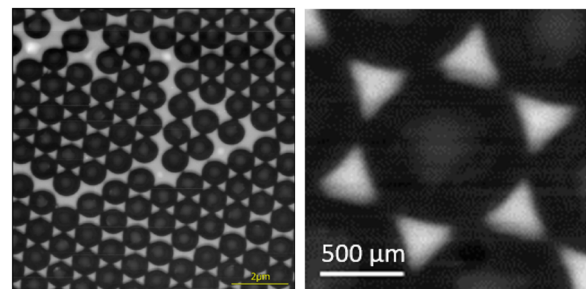
**FIG. 3.** AFM contact mode images of the Au nanoprism sample.

at 633 nm, the calculated contrast $s_{SiO_2}/s_{Si} = 1.25$, which is reasonably close to our measured average contrast of $s_{SiO_2}/s_{Si} = 1.15$ at the second harmonic $n = 3$. This quantity was obtained by taking an average of the optical amplitude value of the top part of the grating compared to the average value of the bottom part of the grating sample. It is important to point out that this type of comparison with theory would not be possible without the use of the stabilization mechanism.

To further test our system, we measured the EM near-field of an array of Au nanoprisms. This sample has been synthesized by nanosphere lithography[15] (NSL) on a sodalime glass substrate, by using polystyrene (PS) nanospheres of diameter D = 1030 nm. An adhesion layer of Cr (about 2 nm thick) and an Au layer of 43 nm are deposited on the PS nanoparticles by magnetron sputtering. The PS nanoparticles are then removed by mechanical stripping with an adhesive tape leaving a honeycomb array of triangular nanoprisms on the substrate (Fig. 3). The lateral size of the nanoprisms is $L = (2 - \sqrt{(3)})$, about 276 nm, the inter-prism distance $d = D/\sqrt{(3)}$, about 595 nm, and the height is about 45 nm.

We used a 1.5 μm diode laser fiber coupled to a reflective collimator as an external source. A calcium fluoride beamsplitter replaced the cube beamsplitter used to measure at optical frequencies. Figure 4 shows the measured signal at the third harmonic. We point out that the AFM topography measurements of the nanoprisms in Fig. 4(a) appear rounded in comparison to the SEM image displayed in Fig. 3. Despite these setbacks, a contrast between glass and Au can clearly be appreciated. The ratio diminishes with respect to the He–Ne laser also in part because of the lower illuminating intensity.

It is important to point out that the stabilization procedure not only allows for a clearer extraction of the optical signal but can also prevent artifacts related to the phase drift in the interferometer. In Fig. 5, we show the measured optical signal at 1500 nm without the stabilization procedure. Due to the instability of the optical path of the interferometer arms, in the image, we clearly observe a contrast inversion between the Au structure and the substrate. This sort of contrast inversion could easily be misinterpreted as originating from contamination of the tip or a real
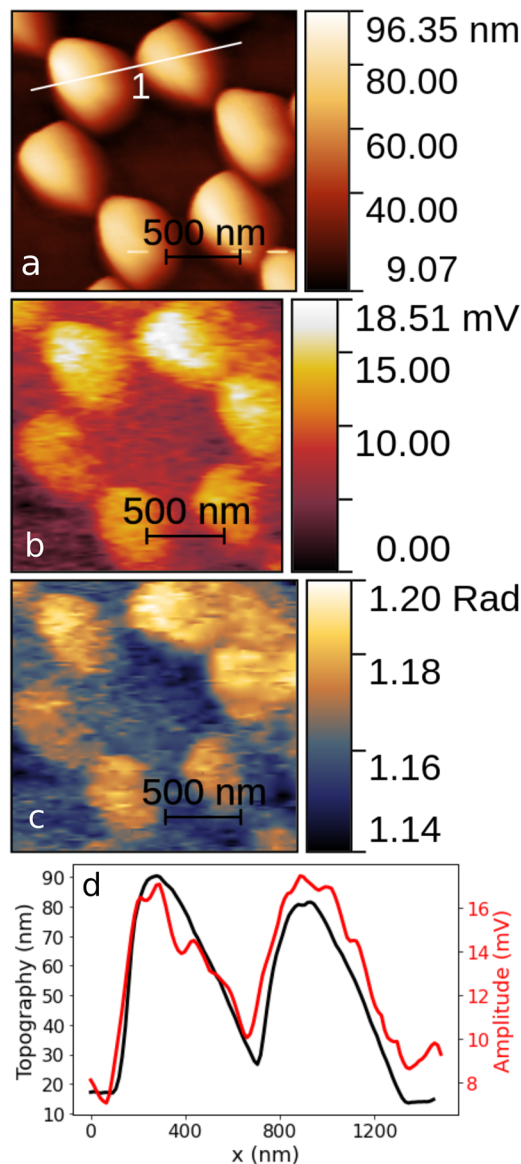
FIG. 4. (a) Topography of the gold nanostructure. (b) Optical amplitude and (c) optical phase measured at 3 Ω with the stabilization mechanism on. (d) Comparison between the topography and optical amplitude profiles along the line shown in (a).
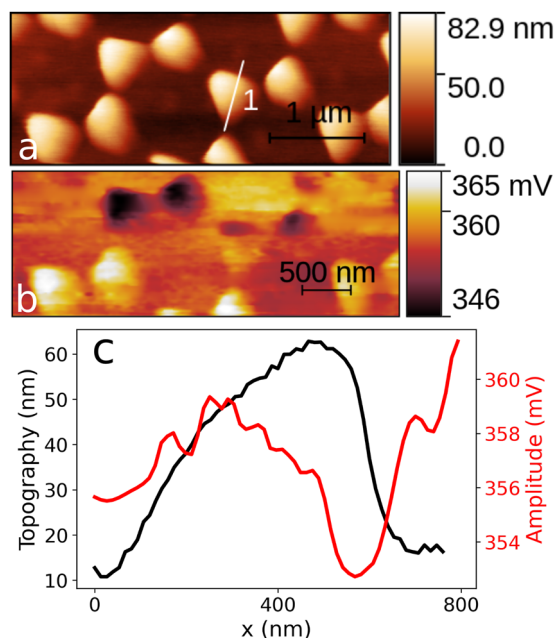
FIG. 5. (a) Topography and (b) optical amplitudes s_2 measured without the stabilizing procedure. (c) Profiles show where contrast inversion occurs over the gold structures.

13 January 2024 00:07:29

change in the dielectric properties of the sample. This type of optical artifact is hampered by our stabilization procedure as shown in Fig. 5.

Before concluding, we point out some assumptions and possible limitations of our stabilization technique. While the use of our stabilization can improve the quality of measurements, acquisition time is increased due to the stabilization time required at each row. The exact amount of time depends on the setup's stability. Typically, the procedure takes about a second at each row; however, ambient conditions of the setup occasionally increase this time. As a reference, for our particular setup and test system, acquisition time was increased by about 20%. Second, note that the observed oscillations due to instabilities are relatively slow, occurring in the order of minutes. Our mechanism assumes that the instabilities that occur during the acquisition of each row can be kept relatively small. In the case of instabilities occurring in smaller time frames or if larger precision is required, our stabilization procedure should be modified to be carried out point by point, at the cost of longer acquisition times.

III. CONCLUSIONS

We presented an interferometric pseudoheterodyne s-SNOM setup and implement an active stabilization mechanism that is capable of eliminating artifacts commonly affecting near-field measurements. By measuring two sidebands of the same harmonic frequency of the AFM tip and implementing a phase control mechanism, the demodulated signal is stabilized, and oscillations in both optical amplitude and phase images are eliminated. We demonstrate our method by acquiring s-SNOM images in a one-dimensional grating composed of Si and SiO_2 and two-dimensional Au nanostructures on glass. For micrometer structures, phase-related artifacts may easily be spotted, while for nanostructures, the troubleshooting is cumbersome and highly non-trivial. The confusion arises because of the similarity between measurement artifacts and the effect of the local variation in material permittivities. Our method, being carried out before each line scan, avoids misleading phase jumps while retaining the true optical contrast of the sample. Our method uses low cost components and open source C++ standard libraries easily adaptable for different s-SNOM configurations. Future improvements to the setup could include a function to automatically choose the correct oscillating driving voltage, V_d, and feedback parameters for a given signal since, for the time being, these must be chosen manually.

SUPPLEMENTARY MATERIAL

See the supplementary material for a derivation of Eq. (1) and an estimation of the resolution of the scattering SNOM setup.

ACKNOWLEDGMENTS

AUTHOR DECLARATIONS

Conflict of Interest

The authors have no conflicts to disclose.

Author Contributions

David Becerril: Conceptualization (equal); Formal analysis (equal); Methodology (equal); Writing – original draft (equal). **Tiziana Cesca**: Methodology (equal); Writing – review & editing (equal). **Giovanni Mattei**: Methodology (equal); Writing – review & editing (equal). **Cecilia Noguez**: Conceptualization (equal); Formal analysis (equal); Methodology (equal); Writing – review & editing (equal). **Giuseppe Pirruccio**: Conceptualization (equal); Formal analysis (equal); Methodology (equal); Writing – review & editing (equal). **Marco Luce**: Conceptualization (equal); Formal analysis (equal); Methodology (equal). **Antonio Cricenti**: Conceptualization (equal); Methodology (equal); Resources (equal); Writing – review & editing (equal).

DATA AVAILABILITY

The data that support the findings of this study are available from the corresponding author upon reasonable request.

REFERENCES

[1] B. Knoll and F. Keilmann, "Enhanced dielectric contrast in scattering-type scanning near-field optical microscopy," Opt. Commun. **182**, 321–328 (2000).

[2] J. M. Stiegler, Y. Abate, A. Cvitkovic, Y. E. Romanyuk, A. J. Huber, S. R. Leone, and R. Hillenbrand, "Nanoscale infrared absorption spectroscopy of individual nanoparticles enabled by scattering-type near-field microscopy," ACS Nano **5**, 6494–6499 (2011).

[3] Y. Li, N. Zhou, A. Raman, and X. Xu, "Three-dimensional mapping of optical near field with scattering SNOM," Opt. Express **23**, 18730–18735 (2015).

[4] V. J. Rao, M. Matthiesen, K. P. Goetz, C. Huck, C. Yim, R. Siris, J. Han, S. Hahn, U. H. F. Bunz, A. Dreuw, G. S. Duesberg, A. Pucci, and J. Zaumseil, "AFM-IR and IR-SNOM for the characterization of small molecule organic semiconductors," J. Phys. Chem. C **124**, 5331–5344 (2020).

[5] X. Chen, D. Hu, R. Mescall, G. You, D. N. Basov, Q. Dai, and M. Liu, "Modern scattering-type scanning near-field optical microscopy for advanced material research," Adv. Mater. **31**, 1804774 (2019).

[6] Y. Martin, S. Rishton, and H. K. Wickramasinghe, "Optical data storage read out at 256 Gbits/in.^{2}," Appl. Phys. Lett. **71**, 1 (1997).

[7] R. Vogelgesang, J. Dorfmüller, R. Esteban, R. T. Weitz, A. Dmitriev, and K. Kern, "Plasmonic nanostructures in aperture-less scanning near-field optical microscopy (ASNOM)," Phys. Status Solidi B **245**, 2255–2260 (2008).

[8] M. Brehm, T. Taubner, R. Hillenbrand, and F. Keilmann, "Infrared spectroscopic mapping of single nanoparticles and viruses at nanoscale resolution," Nano Lett. **6**, 1307–1310 (2006).

[9] N. Ocelic, A. Huber, and R. Hillenbrand, "Pseudoheterodyne detection for background-free near-field spectroscopy," Appl. Phys. Lett. **89**, 101124 (2006).

13 January 2024 00:07:29

[10] A. A. Freschi and J. Frejlich, "Adjustable phase control in stabilized interferometry," Opt. Lett. **20**, 635–637 (1995).

[11] X. G. Xu, L. Gilburd, and G. C. Walker, "Phase stabilized homodyne of infrared scattering type scanning near-field optical microscopy," Appl. Phys. Lett. **105**, 263104 (2014).

[12] M. Xiao, "Theoretical treatment for scattering scanning near-field optical microscopy," J. Opt. Soc. Am. A **14**, 2977–2984 (1997).

[13] S-SNOM stabilization," https://github.com/dbecerril/InterferometerControl, 2022.

[14] D. E. Tranca, S. G. Stanciu, R. Hristu, C. Stoichita, S. A. M. Tofail, and G. A. Stanciu, "High-resolution quantitative determination of dielectric function by using scattering scanning near-field optical microscopy," Sci. Rep. **5**, 11876 (2015).

[15] T. Cesca, N. Michieli, B. Kalinic, I. G. Balasa, R. Rangel-Rojo, J. A. Reyes-Esqueda, and G. Mattei, "Bidimensional ordered plasmonic nanoarrays for nonlinear optics, nanophotonics and biosensing applications," Mater. Sci. Semicond. Process. **92**, 2–9 (2019), part of special issue: Material processing of optical devices and their applications.

13 January 2024 00:07:29